Preprint typeset using LaTeX style emulateapj v. 12/16/11

PROBING THE CIRCUMGALACTIC MEDIUM OF SUBMILLIMETER GALAXIES WITH QSO ABSORPTION SPECTROSCOPY

HAI FU[1] AND COLLABORATORS

ABSTRACT

Submillimeter galaxies (SMGs) are dusty starbursts in the early universe that are likely to evolve into massive ellipticals today. The physical state of the circumgalactic medium of SMGs carries key information to decode massive galaxy formation yet are unexplored observationally. We exploit QSO absorption spectroscopy to probe the diffuse gas around SMGs. We first compile a sample of SMG–QSO pairs with angular separations less than 35″ from *Herschel* surveys. We then use the Very Large Array (VLA) to determine the positions of the *Herschel* sources. Finally, we use near-infrared spectrographs to determine the redshifts of the five VLA-detected SMGs and optical spectrographs to obtain their QSO absorption spectra. Our survey yielded three SMG–QSO pairs with secure redshift identification for both components. The QSO sightlines probe transverse proper distances between 110 and 200 kpc. We detect strong H I Lyα absorption with rest-frame equivalent widths $W_{\rm Ly\alpha} = 1.7-2.0$ Å around all three SMGs. One of the Lyα system shows only 40% absorption at the line center, so it is clearly optically thin ($\log(N_{\rm HI}) < 17$ cm^{-2}) and the high $W_{\rm Ly\alpha}$ is due to line-blending. The high equivalent widths and the line center depths of the other two systems are consistent with optically thick absorbers with $18 < \log(N_{\rm HI}) < 19$ cm^{-2}. However, neither are convincingly optically thick, because our spectral resolution is insufficient to reveal the damping wings of the Lyα line and the low-ionization metal lines commonly associated with optically thick absorbers are buried in the Lyα forest. Compared with the QSOs at $z \sim 2$, our limited sample suggests that SMGs' surrounding media have lower covering fraction of optically thick cool gas between $100 < R_\perp < 200$ kpc.

Keywords: galaxies: halos — quasars: absorption lines — intergalactic medium

1. INTRODUCTION

The first mJy-level submillimeter surveys discovered a population of high-redshift submillimeter-bright galaxies (SMGs), namely, unresolved sources with 850 μm flux density (S_{850}) greater than 3–5 mJy (Smail et al. 1997; Barger et al. 1998; Hughes et al. 1998; Eales et al. 1999). The SMGs are intense starbursts (SFR $\gtrsim 500$ M$_\odot$ yr^{-1}) at a median redshift of $z \sim 2.5$ (Chapman et al. 2005; Wardlow et al. 2011; Yun et al. 2012; Smolčić et al. 2012)[2]. The star formation is dust-enshrouded so that the SMGs emit most of their bolometric luminosity in the far-infrared (FIR). The observed molecular and stellar emission indicate that they are massive gas-rich galaxies ($\sim 10^{11}\,M_\odot$), but the typical halo mass of SMGs remains uncertain, with estimates ranging from 10^{12} to $10^{13}\,M_\odot$. Two lines of evidence suggest that SMGs may inhabit dark matter halos as massive as $\sim 10^{13}\,M_\odot$: (1) their strong clustering strength estimated from either the angular two-point correlation function (e.g., Scott et al. 2006; Weiß et al. 2009) or the cross-correlation function between SMGs and other high-redshift galaxies (e.g., Hickox et al. 2012), and (2) their high stellar mass and the $M_{\rm star}$–$M_{\rm halo}$ relation from abundance matching ($M_{\rm halo} = 6 \times 10^{12}\,M_\odot$ for $M_{\rm star} = 10^{11}\,M_\odot$ at $z = 2$; e.g., Behroozi et al. 2010). But because source blending due to the large beams of single-dish (sub)millimeter telescopes may have significantly elevated the clustering strength (Cowley et al. 2016) and the stellar mass estimates remain uncertain within an order of magnitude (e.g., Hainline et al. 2011; Michałowski et al. 2012; Targett et al. 2012), it is possible that a typical SMG may inhabit much less massive halos ($\sim 10^{12}\,M_\odot$).

SMGs are absent in the local universe and it is commonly thought that they have evolved into the massive ellipticals today (e.g., Blain et al. 2004; Toft et al. 2014). To understand the evolution of SMGs, it is imperative to know how long the observed intense star formation would last. For $10^{13}\,M_\odot$ halos at $z = 2.5$, the total baryonic accretion rate from the mass growth rate of dark matter haloes is $\dot{M}_{\rm gas} \equiv 0.18 \times \dot{M}_{\rm halo} \simeq 1.4 \times 10^3$ M$_\odot$ yr^{-1} (Neistein & Dekel 2008; Bouché et al. 2010). In such massive halos, it is expected that most of the baryons will be shock-heated to the virial temperature of the halo ($\sim 10^7$ K) and the cool gas replenishment timescale is much longer than the gas depletion timescale in such halos (e.g., Dekel & Birnboim 2006; Tacchella et al. 2015). Therefore, the prolific star formation in SMGs should be unsustainable; the SFR would decline with an *e*-folding timescale of only $\sim$200 Myr ($2M_{\rm gas}$/SFR; e.g., Greve et al. 2005; Tacconi et al. 2008; Ivison et al. 2011; Bothwell et al. 2013). At such a rate, the SMGs would become red sequence galaxies in only a Gyr or 5 *e*-folding times[3] (Fu et al. 2013). Such a short transitional time of a significant high-redshift star-forming population might help explain the rapid build-up of the massive end of the red sequence at $z > 1$ (e.g., Ilbert et al. 2013). This makes it unnecessary to invoke any additional quenching mechanisms such as galactic outflows, which can be suppressed in such massive halos (e.g., Singh et al. 2016). On the other hand, if SMGs were in $10^{12}\,M_\odot$ halos, the intense star formation is also unsustainable because the gas accretion rate is only $\sim$110 M$_\odot$ yr^{-1} at $z = 2.5$; but after the starburst phase,

[1] Department of Physics & Astronomy, University of Iowa, Iowa City, IA 52242

[2] The redshift distribution of dusty star-forming galaxies is highly dependent on the selection wavelength (e.g., Casey et al. 2014; Béthermin et al. 2015), here we focus on samples selected between 850 μm and 1 mm.

[3] This is the time it would take to decrease the specific SFR (SFR/$M_{\rm star}$) from $\sim 10^{-9}$ Gyr^{-1} for the SMGs at the observed epoch to $\sim 10^{-11}$ Gyr^{-1} for the red sequence at $z \sim 2$ (Brammer et al. 2009).

Table 1
VLA Observed *Herschel* Sources

Pair Name	RA_{250} (deg)	DEC_{250} (deg)	S_{250} (mJy)	S_{350} (mJy)	S_{500} (mJy)	Int Time (min)	RA_{6GHz} (deg)	DEC_{6GHz} (deg)	S^{peak}_{6GHz} (μJy/bm)	S^{int}_{6GHz} (μJy)
(1)	(2)	(3)	(4)	(5)	(6)	(7)	(8)	(9)	(10)	(11)
HeLMS 0015+0404	3.9286	+4.0715	61.7±6.0	67.8±5.7	54.3±7.2	26.5	3.93038	+4.07262	69.4±6.7	72.4±13.4
HeLMS 0041−0410	10.3541	−4.1679	80.8±6.2	83.0±6.5	43.6±7.0	15.8	···	···	<35.1	···
L6-XMM 0223−0605	35.8056	−6.0860	33.8±2.3	40.3±2.5	24.2±3.5	69.7	···	···	<14.4	···
G09 0918−0039	139.6159	−0.6644	41.1±6.9	49.7±8.1	31.2±9.1	18.9	···	···	<17.7	···
G09 0920+0024	140.2475	+0.4049	35.0±7.0	51.6±8.1	32.0±8.9	22.9	···	···	<18.6	···
NGP 1313+2924	198.4530	+29.4126	59.7±5.6	78.5±6.6	53.6±7.8	17.2	···	···	<42.3	···
NGP 1330+2540	202.5866	+25.6749	49.2±5.8	54.3±6.4	29.3±7.8	18.0	···	···	<15.3	···
NGP 1333+2357	203.3743	+23.9592	30.4±5.4	31.8±6.4	29.1±7.5	55.2	203.37514	+23.95909	20.0±3.0	31.0±8.1
NGP 1335+2805	203.9409	+28.0986	41.7±5.5	49.8±6.4	38.2±7.7	27.6	203.94249	+28.09750	38.3±4.5	51.4±11.0
G15 1413+0058	213.4580	+0.9725	46.6±6.4	52.8±7.7	36.1±8.5	16.2	213.45743	+0.97321	37.3±5.8	37.3±11.6
G15 1435+0110	218.9043	+1.1682	63.0±6.7	63.8±8.0	56.6±8.8	9.2	218.90494	+1.16958	75.6±7.3	89.1±16.0
G15 1450+0026	222.6773	+0.4351	47.5±6.9	47.9±8.1	29.1±8.9	16.3	···	···	<18.0	···
L6-FLS 1712+6001	258.0352	+60.0281	32.3±2.2	34.0±2.4	22.4±3.6	30.1	258.03111	+60.02722	10.8±2.1	10.8±4.2

Note. — Columns (2-6) list the *Herschel* 250 μm positions and the photometry at 250, 350, and 500 μm. Column 7 is the total VLA on-source integration time. Columns (8-9) list the positions of the radio counterparts. Columns (10-11) are the peak flux density in μJy/bm and the integrated flux density in μJy, both of which are derived by fitting an elliptical Gaussian model to the source. The uncertainty of peak flux density is given by the rms noise in the map at the source position, while the uncertainty of the integrated flux density is estimated using the formulae provided by Hopkins et al. (2003), which includes the 1% uncertainty in the VLA flux-density scale at 6 GHz (Perley & Butler 2013).

they will evolve into typical star-forming galaxies instead of red sequence galaxies.

However, could there be enough cool gas in the circumgalactic medium (CGM) around SMGs to fuel a prolonged starburst phase (e.g. Narayanan et al. 2015)? The CGM of coeval QSOs may give us a hint, because they inhabit comparably massive ($\sim 10^{12.6} M_\odot$) halos (White et al. 2012). Contrary to the expected dominance of virialized X-ray plasma, absorption line spectroscopy of a statistical sample of $z \sim 2$ projected QSO pairs reveals the prevalence of cool ($T \sim 10^4$ K), metal-enriched ($Z \geq 0.1 Z_\odot$), and optically thick Lyα absorbers ($N_{\rm HI} \geq 1.6 \times 10^{17}$ cm^{-2}) extending to at least the expected virial radius of 160 kpc (the "Quasar Probing Quasar" [QPQ] project: Hennawi et al. 2006; Hennawi & Prochaska 2007; Prochaska et al. 2013a,b). The high observed covering factor of the cool CGM gas ($\gtrsim 60\%$) in $\sim 10^{12.6} M_\odot$ halos has been compared to predictions from numerical simulations. While several studies found that they cannot reproduce the high covering factor around quasars (Fumagalli et al. 2014; Faucher-Giguère et al. 2015, but see Rahmati et al. 2015), it has been argued that efficient star-formation-driven feedback from accreted satellite galaxies is required to increase the H I covering factor to the observed level, which is only resolved in the highest resolution cosmological zoom simulations (Faucher-Giguere et al. 2016).

The models predict that the covering factor increases with halo mass and is independent of specific SFR, so SMGs are likely to show even higher H I covering factors if there were indeed in 10^{13} $M_\odot$ halos. To test this, we exploit QSO absorption line spectroscopy to probe the CGM of SMGs. We first present the data sets and the method we used to select projected SMG–QSO pairs in § 2. We then describe our followup observations in § 3, including radio interferometer imaging, near-infrared spectroscopy, and optical spectroscopy. We present our analysis and results in § 4, including a comparison between the covering fraction of optically thick gas around SMGs and that of $z \sim 2$ QSOs. A summary is provided in § 5. Throughout we adopt a ΛCDM cosmology with $\Omega_{\rm m} = 0.27$, $\Omega_\Lambda = 0.73$ and $H_0 = 70$ km s^{-1} Mpc^{-1}.

2. SELECTION OF PROJECTED SMG–QSO PAIRS

Because both high-redshift QSOs and SMGs have low surface densities on the sky, we need large samples of both to come up with a sizable sample of projected SMG–QSO pairs with small angular separations. We compiled 464,866 spectroscopically confirmed QSOs from various surveys: primarily, the Sloan Digital Sky Survey (SDSS; Alam et al. 2015), the 2dF QSO Redshift Survey (2QZ; Croom et al. 2004), the AGN and Galaxy Evolution Survey (AGES; Kochanek et al. 2012), and the MMT Hectospec Redshift Survey of 24 μm Sources in the Spitzer First Look Survey (Papovich et al. 2006). Since we select the foreground galaxies that are likely at $z > 2$ (see the next paragraph), we keep only the 102,472 QSOs at $z_{\rm QSO} > 2.5$. The average surface density of background QSOs is thus $\sim 10\,{\rm deg}^{-2}$.

To select the foreground SMGs, we combined source catalogs from a number of wide-area *Herschel* extragalactic surveys: the *Herschel* Multi-tiered Extragalactic Survey (HerMES, 95 deg^2; Oliver et al. 2012; Wang et al. 2014), the *Herschel* Astrophysical Terahertz Large Area Survey (H-ATLAS, 600 deg^2; Eales et al. 2010; Valiante et al. 2016), the *Herschel* Large Mode Survey (HeLMS, 301 deg^2; Oliver et al. 2012; Clarke & et al. 2016; Asboth et al. 2016; Nayyeri et al. 2016), the *Herschel* Stripe 82 Survey (HerS, 79 deg^2; Viero et al. 2014). All of these surveys used SPIRE (Spectral and Photometric Imaging Receiver; Griffin et al. 2010) to image the sky at 250, 350, and 500 μm and the combined xID250[4] catalog contain 1,586,047 sources covering a total of 767 deg^2 (HerS and HeLMS fields overlap by 10 deg^2). However, most *Herschel* sources are not SMGs. They are mostly less luminous dusty star-forming galaxies at $z < 2$ (Casey et al. 2012). To select *Herschel* sources that are likely *bona fide* SMGs, we chose only the subsample that satisfies the following criteria: (1) flux densities peak at 350 μm ($S_{250} < S_{350}$ and $S_{500} < S_{350}$; i.e., "350μm peakers"), (2) $S_{500} > 20$ mJy, and (3) $>3\sigma$ detections in all three SPIRE bands. Criterion 1 is essentially a photometric redshift selection because emission

[4] 250, 350 and 500 μm fluxes were all extracted at source positions detected on the 250 μm map (e.g., Roseboom et al. 2010; Rigby et al. 2011).

from dusts at $T = 35$ K would peak at 350 μm if redshifted to $z \sim 2.5 \pm 0.8$. In addition, the blind CO survey of the brightest 350 μm peakers ($S_{350} \geq 115$ mJy) has shown a strikingly similar redshift distribution as 850 μm-selected SMGs (Harris et al. 2012), even though most of these bright sources are strongly lensed. Criterion 2 is introduced to ensure that the Rayleigh-Jeans extrapolation would give $S_{850} > 3$ mJy, the classic definition of an SMG, given a typical power-law slope of 3.5 for a modified blackbody with a frequency-dependent absorption cross section ($\kappa \propto \nu^{1.5}$). Criterion 3 ensures that all of the sources we considered are statistically significant. This is necessary because the image depth varies substantially from field to field, ranging from $\sigma_{500} = 15$ mJy beam^{-1} for the large HeLMS and HerS fields (confusion noise included; Oliver et al. 2012; Viero et al. 2014) to confusion limited with $\sigma_{500} = 6.8$ mJy beam^{-1} for the deeper HerMES fields (Nguyen et al. 2010). Of course, our crude color plus flux selection is not completely reliable, but it has weeded out most of the dusty star-forming galaxies that are not SMGs. Only 70,823 *Herschel* sources remained after this selection. The average surface density of 92 deg^{-2} is five times lower than the observed 870 μm source count above $S_{870} \gtrsim 3$ mJy ($\sim$500 deg^{-2}; Weiß et al. 2009; Coppin et al. 2006). This is not surprising given that almost half of the total *Herschel* area is only 10-20% complete at $S_{500} = 20$ mJy. Note that this incompleteness is not a concern for our purpose.

We identified 230 projected SMG–QSO pairs with separations[5] between $5'' \leq \theta_{250} \leq 36''$ by cross-matching the QSO and SMG subsamples described above. The corresponding impact parameters ($R_\perp$)[6] are between $40 < R_\perp < 300$ kpc for $z_{\rm SMG} = 2.5$. These QSO sightlines thus probe out to $\sim$1.5 virial radii of 10^{13} $M_\odot$ halos ($r_{\rm vir} = 200$ kpc at $z = 2.5$). Because the typical positional uncertainty of the *Herschel* sources is $\sim 5''$, the $5''$ lower limit on the angular separation is imposed as an attempt to avoid FIR-luminous QSOs, i.e., the QSOs are the SMGs themselves. The FIR-luminous QSOs are interesting on their own right and they will be discussed elsewhere. As we will show in § 4.1, one of the six VLA-detected *Herschel* sources still turned out to be a FIR-luminous QSO, meaning that the positional uncertainty has been underestimated. Through visual inspection of the QSO spectra, we further excluded 31 pairs whose QSOs exhibit strong broad absorption lines (BALs; this makes them unsuitable for absorption line work), have wrong redshifts, or are misclassified. Therefore, our final sample includes 199 pairs, among which 90/163 QSOs have SDSS $g \leq 21/22$.

3. FOLLOWUP OBSERVATIONS

Extensive followup observations are needed to perform the absorption analysis of SMGs. Identifying the absorption features in the spectrum of the background QSO requires a precise redshift for the foreground SMG. But the angular resolution of *Herschel* (FWHM = $18''/25''/36''$ at 250/350/500 μm) precludes longslit spectroscopic observations with typical slit width of $1''$. To obtain more accurate positions and to remove blended sources, we exploit interferometer observations of 15 SMG–QSO pairs with the Karl G. Jansky Very Large Array (VLA). Furthermore, once the positions are determined with sub-arcsec accuracy, we need to determine the spectroscopic redshifts of the SMGs with near-IR spectrographs by targeting rest-frame optical lines that suffers less dust extinction than rest-frame UV lines. Finally, a high S/N optical/near-UV spectrum of the background QSO is needed to detect the UV absorption lines imprinted by the diffuse medium around the SMGs. Below we describe these observations in more details.

3.1. *SMG Identification with the VLA*

FIR-luminous galaxies like our *Herschel* sources are expected to be luminous in the radio wavelengths, according to the FIR-radio correlation (Helou et al. 1985; Condon 1992; Ivison et al. 2010). We can thus obtain better positions for the *Herschel* sources by identifying the radio counterparts with interferometers. We observed 15 SMG–QSO pairs with the VLA in the B configuration with the C-band (6 GHz) receivers (program ID: 15A-266). The sample was selected randomly from the 90 SMG–QSO pairs with QSOs brighter than $g \leq 21$, excluding those with $\theta_{250} > 30''$. We later realized that two of the VLA targets in the HeLMS field are likely spurious detections because of Galactic cirrus (Clarke et al. in prep.), so we excluded them in this discussion. Table 1 lists the *Herschel* positions and photometry of the final VLA sample. The receivers have a total bandwidth of 4 GHz at a central frequency of 5.9985 GHz. The targets were selected from six different extragalactic fields. To maximize the observing efficiency, we grouped the targets with their R.A. into five scheduling blocks (SBs) of 0.8 to 3.1 hours. A nearby unresolved calibrator was observed every $\sim$10 min. Depending on the R.A. of the targets, 3C 48, 3C 286, or 3C 295 was observed for bandpass and flux-density calibration. The entire program took 8.3 hrs of VLA time. The on-source integration time ranges from 9 to 70 minutes, allocated based on the 6 GHz flux density estimated from fitting the *Herschel* photometry with the SED template of a well-studied lensed SMG at $z = 2.3259$ (SMM J2135-0102, aka. the "Eyelash"; Swinbank et al. 2010).

The observations were calibrated using the Common Astronomical Software Applications (CASA) package. We used the VLA pipeline to perform basic flagging and calibration. Additional flagging was performed whenever necessary by inspecting the visibility data. We used the self-calibration technique with bright sources within the primary beam to improve the calibration for four fields: HeLMS 0015+0404, HeLMS 0041–0410, L6-XMM 0223–0605, and NGP 1313+2924. For imaging and deconvolution, we used the standard CASA task CLEAN with "natural" weighting to achieve the best sensitivity. The resulting restoring beams are on average $1\farcs5 \times 1\farcs2$ FWHM. The rms image noise level ranges from 2.1 to 14.1 μJy beam^{-1}, with a mean of 6 μJy beam^{-1}. This measured noise is consistent with thermal noise using natural weighting of the visibility data, except for maps contaminated by confusion from the sidelobes of uncleaned sources lying outside the cleaned image.

We will present the results in § 4.1, but here is a summary: The VLA detected six of the 13 SMGs; For one of those, NGP 1335+2805, the QSO at $z = 2.973$ itself is responsible for the FIR emission, so we excluded it from subsequent spectroscopic observations.

3.2. *Near-IR Spectroscopy of the VLA-detected SMGs*

With the VLA positions that are accurate to $\lesssim 0.1''$, we carried out a redshift survey for the five VLA-detected

[5] θ_{250} is measured between the *Herschel* 250 μm position and the optical position of the QSO.

[6] The impact parameter is defined as the transverse proper distance at the redshift of the foreground SMG, which equals the angular diameter distance of the SMG multiplied by the angular separation on sky ($R_\perp = D_{\rm A}(z) \times \theta$).

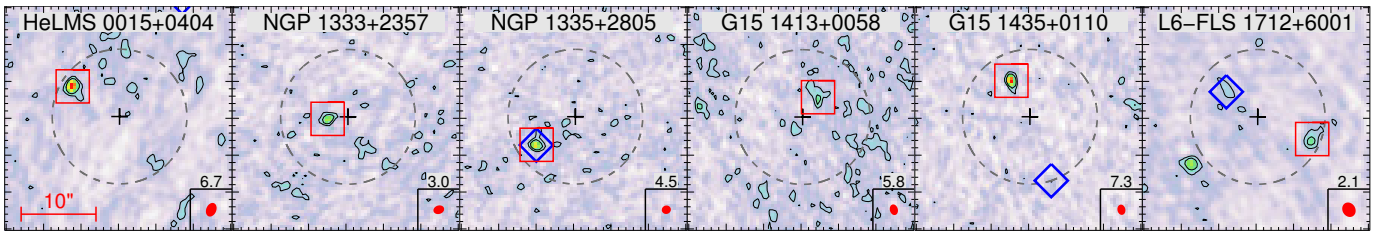

Figure 1. VLA 6 GHz continuum maps for the six VLA-identified SMGs. Each image is $30'' \times 30''$ centered on the *Herschel* position. The restoring beam of each map is plotted as the red ellipse at the lower right corner, above which the 1σ noise level is labeled in units of μJy beam^{-1}. The cross and the dashed circle indicate the *Herschel* positions and the $18''$ FWHM of the 250 μm PSF. The red square highlights the detected radio source within the *Herschel* FWHM. The blue diamond marks the optical position of the QSO, if it is within the displayed region. The contours are at (+2, +4)σ ($\bar{\sigma} = 4.9\,\mu$Jy beam^{-1}). Major tickmarks are spaced in $5''$ intervals. N is up and E is left for all panels.

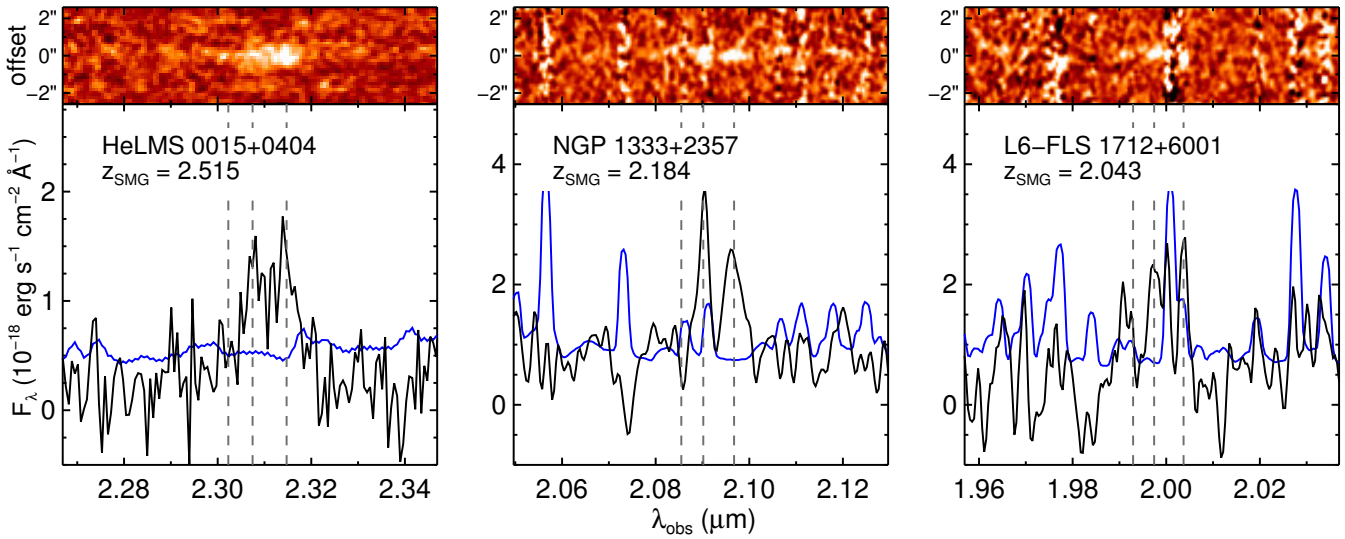

Figure 2. Near-infrared spectra of the VLA-identified SMGs. The top panel shows the coadded 2D spectrum. The vertical axis is along the spatial direction, and is centered on the SMG location. The bottom panel shows the flux-calibrated 1D spectrum (*black*) and its 1σ uncertainty (*blue*). Wavelengths affected by strong sky lines show large errors. The dashed lines indicate the redshifted Hα λ6563 and [N II] $\lambda\lambda$6548,6583 lines.

SMG–QSO pairs with NIR spectrographs. We observed G15 1435+0110, L6-FLS 1712+6001, and NGP 1333+2357 with the LUCI-1 spectrograph (LBT NIR-Spectroscopic Utility with Camera and Integral-Field Unit; Seifert et al. 2003) on the Large Binocular Telescope (LBT) on 2015 Apr 14. We used the 200 l/mm H+K grating at $\lambda_c = 1.93$ μm and the N1.8 camera ($0\farcs25$ per pixel) to obtain a spectral range between 1.5 and 2.3 μm. The $1''$-wide $4'$-long slit is centered on the VLA-determined SMG position, and the slit P.A. is chosen to obtain the QSO spectrum simultaneously. The spectral resolution (R) is $\sim$940 in H-band and $\sim$1290 in K-band. We obtained 32$\times$ 120 s exposures for each target. Between exposures, we dithered along the slit among six dithering positions distributed within $40''$. Atmospheric transparency varied dramatically during the night and no telluric star was observed. So we used the telluric star observation from the previous night for an approximate telluric and flux calibration.

We observed HeLMS 0015+0404 and G15 1413+0058 with the Gemini near-infrared spectrograph (GNIRS; Elias et al. 2006) in the queue mode (program IDs: GN-2015B-Q-46, GN-2016A-Q-41). We used the cross-dispersing prism with the 31.7 l/mm grating and the short camera to obtain a complete spectral coverage between 0.85-2.5 μm. With the $0\farcs68$ short slit, the spectral resolution is $R \sim 750$ across all orders. We obtained 14$\times$ 300 s exposures for HeLMS 0015+0404 on 2015 Aug 9, Aug 12, and Oct 18, and 24$\times$ 115 s exposures for G15 1413+0058 on 2016 May 20. We dithered by $3''$ along the $7''$-slit between exposures.

Data reduction was carried out with a modified version of `LONGSLIT_REDUCE` (Becker et al. 2009) for LUCI-1 by F. Bian (Bian et al. 2010), a modified version of Spextool (Cushing et al. 2004; Vacca et al. 2003) for GNIRS by Katelyn Allers (private communication), and the original version of `LONGSLIT_REDUCE` for NIRSPEC (Becker et al. 2009). These IDL packages carry out the standard data reduction steps for longslit near-IR spectra: flat-fielding, wavelength calibration with sky lines, pairwise sky subtraction, residual sky removal, shifting and coadding, spectral extraction, telluric correction, and flux calibration.

3.3. *Optical Spectroscopy of the Background QSOs*

Although optical spectra exist for all of the QSOs in our sample, most of them do not have the necessary wavelength coverage or sufficient S/N for absorption line analysis. So we obtained new optical spectra for the three background QSOs that are associated with the spectroscopically identified SMGs. We observed L6-FLS 1712+6001 on 2015 Jun 13 and HeLMS 0015+0404 and NGP 1333+2357 on 2016 Jan 9 with the Low Resolution Imaging Spectrometer (LRIS; Oke et al. 1995) on the Keck I telescope. We used the $1''$ longslit and the 560 Dichroic for both runs. For the former run, we used the 400/3400 Grism on the blue side ($R \simeq 540$) and the 400/8500 grating tilted to a central wavelength of $\lambda_c = 8300$ Å on the red side. For the latter run, we used the 600/4000 Grism on the

blue side ($R \simeq 920$) and the 600/7500 grating at $\lambda_c = 7407$ Å on the red side. With the chosen dispersive elements, the spectral resolutions in FWHM are ∼4-7 Å and ∼5-7 Å for the blue and red spectra, respectively. The total integration time for each source ranged between 30 min and 40 min. Conditions were non-photometric for both nights.

We reduced the raw data with XIDL[7], an IDL data reduction package for a number of spectrographs written by two of us (JXP and JH). The pipeline follows the standard data reduction steps and reduces the blue and red channels separately. It begins by subtracting a super bias from the raw CCD frames, tracing the slit profiles using flat fields, and deriving the 2D wavelength solution for each slit using the arcs. Then it flat-fields each slit and rejects cosmic-rays, identifies objects automatically in the slit, and builds the 2D bspline super sky model without rectification (Kelson 2003). After subtracting the super sky model, it performs optimal 1D extraction based on the spatial profile of the QSO (Horne 1986). Finally, it removes instrument flexure using isolated sky lines, performs heliocentric correction, and does flux calibration.

4. RESULTS

4.1. *Radio Detections and Astrometry*

We targeted the *Herschel* sources in 13 SMG–QSO pairs with the VLA and made six clear detections (46% detection rate). Figure 1 shows the VLA detections and Table 1 lists the 6 GHz positions and flux density measurements for the detections and 3σ upper limits on the non-detections. The VLA revealed five genuine SMG–QSO pairs (HeLMS 0015+0404, NGP 1333+2357, G15 1413+0058, G15 1435+0110, L6-FLS 1712+6001) and one FIR-luminous QSO (NGP 1335+2805).

The VLA-detected SMGs have 6 GHz peak flux densities between 11 and 76 μJy with a mean of ∼40 μJy. For these detections, there is a clear positive correlation between the observed flux densities at 6 GHz and 500 μm, as expected from the FIR-radio correlation convolved with a redshift distribution. The 54% non-detection rate is not surprising given the uncertainties in the predicted 6 GHz flux density and the fact that the sensitivity of radio data fluctuates substantially around the theoretical prediction because of confusion sources and weather. The 3σ upper limits from the non-detections all lie within 0.2 dex of the above correlation, suggesting that they could have been detected with deeper data.

The offsets between the *Herschel* positions and the VLA positions range between 2.7″ and 7.9″. The average offset of 5.6″ is comparable to the reported 5″ 95%-ile positional uncertainty of *Herschel* catalogs. However, 2/3 of the sources show offset greater than 5″, indicating that the uncertainty is underestimated. As a result, some of the pairs in the parent sample (§ 2) that have small angular separations ($\theta_{250} \lesssim 8''$) may turn out to be single sources, i.e., QSOs that are FIR-luminous. In our VLA-detected sample, NGP 1335+2805, with $\theta_{250} = 6.5''$, is the only such case (see Fig. 1), since the VLA position is coincident with the optical quasar position within the astrometry uncertainty of 0.1″. But on the other hand, the SMG in L6-FLS 1712+6001 is a separate source from the QSO, despite its even smaller separation ($\theta_{250} = 5.4''$).

4.2. *Physical Properties of the SMGs*

We obtained deep near-IR spectra for the five VLA-detected SMGs whose spectroscopic redshifts are unknown. We detected Hα and [N II] lines from three of the five sources, enabling accurate determination of the spectroscopic redshifts (Fig. 2). The two remaining sources, G15 1413+0058 and G15 1435+0110, show near-IR continuum emission with neither emission lines nor stellar absorption features. It is possible that the emission lines either fall into one of the telluric absorption bands or are simply outside of the spectral range. Our redshift success rate is thus 60%, comparable to previous redshift surveys of SMGs in the optical (e.g., Chapman et al. 2005; Casey et al. 2011).

With the photometry from *Herschel* and the VLA and spectroscopic redshifts, we can estimate the total rest-frame 8–1000 μm luminosity ($L_{\rm IR}$) and the IR-to-radio luminosity ratio ($q_{\rm IR}$). We fit the *Herschel* photometry with a modified blackbody at the spectroscopic redshift, with β fixed to 1.5). We find that they are all Ultra-Luminous IR Galaxies (ULIRGs) with $L_{\rm IR} > 10^{12.5}\,L_\odot$ and SFR$_{\rm IR}$ = 470-1500 M$_\odot$ yr^{-1}. The SFR is estimated from $L_{\rm IR}$ using the calibration of Murphy et al. (2011) for a Kroupa (2002) initial mass function:

$$\mathrm{SFR}/M_\odot\ \mathrm{yr}^{-1} = 1.5\times10^{-10}\,L_{\rm IR}/L_\odot. \quad (1)$$

The extrapolated 850 μm flux densities range between $7 \leq S_{850} \leq 18$ mJy, confirming that they are *bona fide* SMGs.

The IR-to-radio luminosity/flux ratio is estimated using the following equation (Helou et al. 1985; Ivison et al. 2010):

$$q_{\rm IR} = \log\frac{S_{\rm IR}/3.75\times10^{12}\ \mathrm{W\ m^{-2}}}{S_{1.4\rm GHz}/\mathrm{W\ m^{-2}\ Hz^{-1}}} \quad (2)$$

where $S_{\rm IR}$ is rest-frame integrated 8-1000 μm flux and $S_{1.4\rm GHz}$ is the rest-frame 1.4 GHz flux density[8]. The former is from the modified blackbody fit to the FIR SED, and the latter is converted from the observed 6 GHz flux densities assuming a typical synchrotron slope ($S_\nu \propto \nu^{-0.8}$). The three SMGs show $2.1 \leq q_{\rm IR} \leq 2.6$, consistent with the observed radio-IR correlation for *Herschel* sources ($q_{\rm IR} = 2.4 \pm 0.5$; Ivison et al. 2010). This indicates that our radio-detected sample is not biased to radio-loud AGNs.

4.3. *Absorption Line Systems*

We searched for H I Lyα absorption from the SMGs in the QSO spectra within ±600 km s^{-1} of the systemic redshifts. The search window is chosen because the halo escape velocity is 610 km s^{-1} at the virial radius ($R_{\rm vir}$ = 230 kpc) of a $10^{13}\,M_\odot$ NFW halo at $z = 2$. Strong Lyα absorption lines are detected in all three systems (Fig. 3). We report their rest-frame equivalent widths (EWs; $W_{\rm Ly\alpha}$) in Table 2. As we have found in our earlier QSO absorption line studies, systematic error associated with continuum placement and line blending generally dominates the statistical error of the QSO spectra. So we estimate the error of $W_{\rm Ly\alpha}$ assuming 10% error in the continuum placement. From our best-fit Gaussians to the absorption profiles (Fig. 3), we find that all three systems show strong Lyα absorption lines with $W_{\rm Ly\alpha} = 1.7-2.0$ Å.

Because of the large uncertainty ($\delta z \simeq 0.8$) in the photometric redshifts from our initial selection of SMGs from the *Herschel* photometry, in some cases the H I Lyα absorption

[7] http://www.ucolick.org/∼xavier/IDL/

[8] This flux ratio is equivalent to the luminosity ratio defined in Kovács et al. (2006).

Table 2
Redshifts and Absorption Line Measurements

Pair Name	SMG (J2000)	$z_{\rm SMG}$	$\log(L_{\rm IR})$ ($L_\odot$)	$q_{\rm IR}$	QSO (J2000)	$z_{\rm QSO}$	$\theta_{\rm 6GHz}$ ($''$)	$R_\perp$ (kpc)	$W_{\rm Ly\alpha}$ (Å)	classification
HeLMS 0015+0404	J001543.29+040421.4	2.515	13.1	2.1	J001542.31+040433.5	3.256	19.0	157	2.0 ± 0.2	ambiguous
NGP 1333+2357	J133330.03+235732.7	2.184	12.6	2.3	J133330.36+235709.9	3.108	23.3	198	1.7 ± 0.2	ambiguous
L6-FLS 1712+6001	J171207.47+600138.0	2.043	12.6	2.6	J171209.00+600144.4	2.821	13.1	112	2.9 ± 0.5	thin

from the SMG in the QSO spectrum may lie within the QSO Lyβ forest. This will be the case if $z_{\rm QSO}-z_{\rm SMG}\gtrsim 0.5$. All three of our pairs fall in this category, so contamination from Lyβ lines in systems in the Lyα forest is a concern. However, assuming the detected absorption to be Lyβ in each case, we searched for the corresponding Lyα lines but did not find any, indicating that Lyβ contamination is not a serious issue for these systems.

We also searched for the strongest metal lines commonly observed in optically thick absorption systems (e.g., Hennawi & Prochaska 2013): Si II λ1260,1304,1527, O I λ1302, C II λ1335, Si IV λ1394,1403, C IV λ1548,1551, Fe II λ1608,2383,2600, Al II λ1671, and Mg II λ2796, 2804. Most of these lines are not detected in any of the systems, so we only show the possible detections of C II and Si IV lines in Fig. 3. In the following, we discuss the systems individually:

- HeLMS 0015+0404 ($z_{\rm SMG}=2.515, z_{\rm QSO}=3.256, R_\perp=157$ kpc): This system shows a strong Lyα absorption at +504 km s^{-1} with $W_{\rm Ly\alpha}=2.0\pm0.2$ Å. There is also a C II absorption at +400 km s^{-1} ($W_{\rm CII}=1.2$ Å). Given these measurements, one would have concluded that this is an optically thick absorber with $N_{\rm HI}\sim10^{19}$ cm^{-2} if the absorption is dominated by a single component. The column density is estimated from the theoretical curve of growth where $W_{\rm Ly\alpha}=7.3\,(N_{\rm HI}/10^{20}\ {\rm cm}^{-2})^{0.5}$ Å for $N_{\rm HI}>10^{18}$ cm^{-2}, the regime where the relation is insensitive to the b-parameter (Mo et al. 2010, §16.4.4). However, the C II absorption could be a false positive, because it is buried in the Lyα forest and we did not detect other low-ionization metal lines to support the C II detection. Without solid detections of strong metal lines and the detection of the damping wings in Lyα, we cannot conclude that the absorber is optically thick based on current data because the high $W_{\rm Ly\alpha}$ could be due to line blending. We therefore classify this system as ambiguous.

- NGP 1333+2357 ($z_{\rm SMG}=2.184, z_{\rm QSO}=3.108, R_\perp=198$ kpc): This system shows a strong Lyα absorption at –34 km s^{-1} with $W_{\rm Ly\alpha}=1.7\pm0.2$ Å. The C II and Si IV absorption profiles are distinctly different: there appear to be two strong absorption components on both sides of the H I absorption but the metal absorption is very weak at the velocity of the H I Lyα. The mismatch in velocity profiles indicates that the metal lines are spurious. Like the previous case, this system is ambiguous.

- L6-FLS 1712+6001 ($z_{\rm SMG}=2.043, z_{\rm QSO}=2.821, R_\perp=112$ kpc): There is a strong Lyα absorption at +200 km s^{-1} with $W_{\rm Ly\alpha}=2.9\pm0.5$ Å. Despite the high EW, this system is unlikely optically thick because the line center drops only to 40% of the continuum intensity. The associated low-ionization metal lines are either very weak ($W\lesssim0.1$ Å) or completely absent. Hence, we classify this system as optically thin.

In summary, we have identified one clearly optically thin case and two ambiguous cases with three QSO sight-lines covering impact parameters between $100<R_\perp<200$ kpc around SMGs at $2.0<z<2.6$.

4.4. *Comparison with the CGM around QSOs*

The CGM of high redshift QSOs is $\gtrsim$60% filled by H I absorbers that are optically thick at the Lyman limit. The high H I covering fraction extends to at least the expected virial radius of $\sim$160 kpc (Hennawi et al. 2006; Prochaska et al. 2013a,b). In Figure 4, we compare (1) the SMG sample distribution with the QSOs from the QPQ project, and (2) the covering fraction of optically thick H I gas around SMGs with that around QSOs. The two samples overlap nicely in the plane of foreground redshift vs. impact parameter: the SMGs cover the same redshift range as the QSOs in the intermediate impact parameter range between 100 and 200 kpc. We calculate the 1σ binomial confidence intervals of the optically thick fraction using the quantiles of the beta distribution (Cameron 2011). Because there is no convincingly optically thick absorber among the three systems we analyzed, our 1σ confidence interval of the covering fraction is 4.2–36.9%. For a fair comparison, we consider all of the QSO sightlines with $100<R_\perp<200$ kpc from QPQ and we find the H I covering fraction is 64^{+7}_{-9}% for 21 optically thick systems among 33 systems. Despite our small sample, the 1σ upper limit is 3σ below the best-estimated covering fraction around QSOs. Therefore, the surrounding medium of SMGs seems more deprived of cool gas than that of QSOs at $z\sim2$, suggesting that the star formation cannot last longer than the $\sim$200 Myr timescale to exhaust the gas in the disk. This conclusion is clearly limited by the small sample size. A more robust comparison awaits a larger sample of spectroscopically confirmed SMG–QSO pairs.

5. SUMMARY AND CONCLUSIONS

THIS SECTION STILL NEEDS TO BE WRITTEN.

We thank K. Mooley and D. Perley for taking the LRIS spectrum of L6-FLS 1712+6001 and D. Ludovici for helping with the VLA data calibration. The National Radio Astronomy Observatory is a facility of the National Science Foundation operated under cooperative agreement by Associated Universities, Inc. Support for this work was provided by the NSF through award GSSP SOSPA3-016 from the NRAO. H.F., D.M., and J.I. acknowledge supports from NASA JPL award 1495624 and University of Iowa funds. The authors wish to recognize and acknowledge the very significant cultural role and reverence that the summit of Mauna Kea has

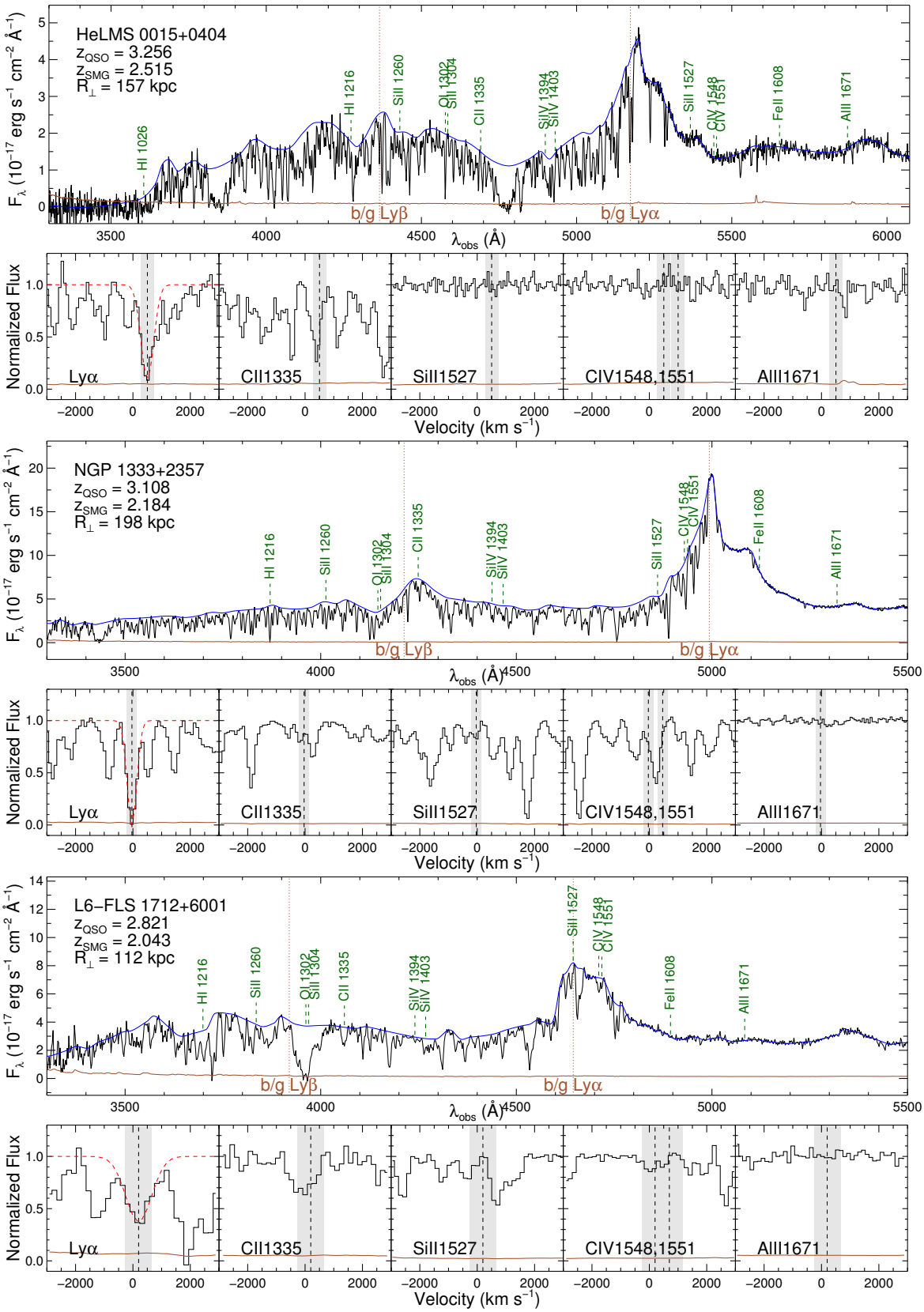

Figure 3. Optical spectra of the background QSOs in the three spectroscopically identified SMG–QSO pairs. The black curve shows the observed flux-calibrated spectrum, while the blue curve shows the continuum model used to normalize the spectrum. The expected locations of absorption lines due to the foreground SMG are marked by green dashed lines. Below the full spectrum, we also show the velocity profiles for the H I Lyα and a number of common metal absorption lines. All panels show the region $\pm$3000 km s^{-1} around the systemic redshifts of the foreground SMGs. In the first panel, we show a Gaussian fit to the strongest H I Lyα absorption line within our search window of $\pm$600 km s^{-1}. The vertical dashed line shows the centroid velocity and the gray shaded region highlights the $\pm1\sigma$ width of the best-fit Gaussian. Both components of the C IV doublet are highlighted.

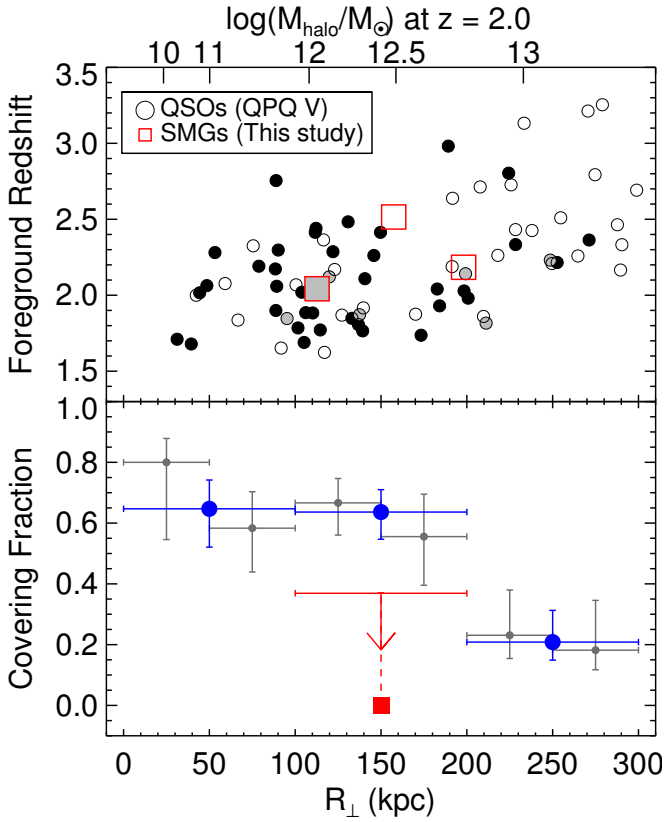

Figure 4. *Top:* Sample distributions in foreground redshift vs. impact parameter. The red squares and the black circles show the SMGs from this study and the QSOs from the QPQ survey (Prochaska et al. 2013a), respectively. The black-filled, gray-filled, and open symbols correspond to systems that are optically thick, optically thin, and ambiguous at the Lyman limit, respectively. The top axis indicates the virial radii of dark matter halos at $z = 2$ from 10^{10} to $10^{13}\,M_{\odot}$. *Bottom:* The covering fraction of optically thick gas around SMGs (*red square with a downward arrow*: our 1σ upper limit) vs. impact parameter, compared to that around QSOs from the QPQ survey (*blue/gray circles* with error bars; Prochaska et al. 2013a). The blue and gray circles are estimates of the covering fraction based on 100 kpc-wide bins and 50 kpc-wide bins, respectively. Our sample probes similar ranges of redshifts and impact parameters as the QPQ QSOs but shows less optically thick absorbers.

always had within the indigenous Hawaiian community. We are most fortunate to have the opportunity to conduct observations from this mountain.

Facilities: Herschel, Sloan, VLA, Keck/LRIS, LBT/LUCI-1, Gemini/GNIRS

REFERENCES

Alam, S., Albareti, F. D., Allende Prieto, C., et al. 2015, ApJS, 219, 12
Asboth, V., Conley, A., Sayers, J., et al. 2016, ArXiv e-prints
Barger, A. J., Cowie, L. L., Sanders, D. B., et al. 1998, Nature, 394, 248
Becker, G. D., Rauch, M., & Sargent, W. L. W. 2009, ApJ, 698, 1010
Behroozi, P. S., Conroy, C., & Wechsler, R. H. 2010, ApJ, 717, 379
Béthermin, M., De Breuck, C., Sargent, M., & Daddi, E. 2015, A&A, 576, L9
Bian, F., Fan, X., Bechtold, J., et al. 2010, ApJ, 725, 1877
Blain, A. W., Chapman, S. C., Smail, I., & Ivison, R. 2004, ApJ, 611, 725
Bothwell, M. S., Smail, I., Chapman, S. C., et al. 2013, MNRAS, 429, 3047
Bouché, N., Dekel, A., Genzel, R., et al. 2010, ApJ, 718, 1001
Brammer, G. B., Whitaker, K. E., van Dokkum, P. G., et al. 2009, ApJ, 706, L173
Cameron, E. 2011, PASA, 28, 128
Casey, C. M., Chapman, S. C., Smail, I., et al. 2011, MNRAS, 411, 2739
Casey, C. M., Narayanan, D., & Cooray, A. 2014, Phys. Rep., 541, 45
Casey, C. M., Berta, S., Béthermin, M., et al. 2012, ApJ, 761, 140
Chapman, S. C., Blain, A. W., Smail, I., & Ivison, R. J. 2005, ApJ, 622, 772
Clarke, C., & et al. 2016, MNRAS, in prep.
Condon, J. J. 1992, ARA&A, 30, 575
Coppin, K., Chapin, E. L., Mortier, A. M. J., et al. 2006, MNRAS, 372, 1621
Cowley, W. I., Lacey, C. G., Baugh, C. M., & Cole, S. 2016, MNRAS
Croom, S. M., Smith, R. J., Boyle, B. J., et al. 2004, MNRAS, 349, 1397
Cushing, M. C., Vacca, W. D., & Rayner, J. T. 2004, PASP, 116, 362
Dekel, A., & Birnboim, Y. 2006, MNRAS, 368, 2
Eales, S., Lilly, S., Gear, W., et al. 1999, ApJ, 515, 518
Eales, S. A., Raymond, G., Roseboom, I. G., et al. 2010, A&A, 518, L23
Elias, J. H., Joyce, R. R., Liang, M., et al. 2006, in Proc. SPIE, Vol. 6269, Society of Photo-Optical Instrumentation Engineers (SPIE) Conference Series, 62694C
Faucher-Giguere, C.-A., Feldmann, R., Quataert, E., et al. 2016, ArXiv e-prints
Faucher-Giguère, C.-A., Hopkins, P. F., Kereš, D., et al. 2015, MNRAS, 449, 987
Fu, H., Cooray, A., Feruglio, C., et al. 2013, Nature, 498, 338
Fumagalli, M., Hennawi, J. F., Prochaska, J. X., et al. 2014, ApJ, 780, 74
Greve, T. R., Bertoldi, F., Smail, I., et al. 2005, MNRAS, 359, 1165
Griffin, M. J., Abergel, A., Abreu, A., et al. 2010, A&A, 518, L3
Hainline, L. J., Blain, A. W., Smail, I., et al. 2011, ApJ, 740, 96
Harris, A. I., Baker, A. J., Frayer, D. T., et al. 2012, ApJ, 752, 152
Helou, G., Soifer, B. T., & Rowan-Robinson, M. 1985, ApJ, 298, L7
Hennawi, J. F., & Prochaska, J. X. 2007, ApJ, 655, 735
—. 2013, ApJ, 766, 58
Hennawi, J. F., Prochaska, J. X., Burles, S., et al. 2006, ApJ, 651, 61
Hickox, R. C., Wardlow, J. L., Smail, I., et al. 2012, MNRAS, 421, 284
Hopkins, A. M., Afonso, J., Chan, B., et al. 2003, AJ, 125, 465
Horne, K. 1986, PASP, 98, 609
Hughes, D. H., Serjeant, S., Dunlop, J., et al. 1998, Nature, 394, 241
Ilbert, O., McCracken, H. J., Le Fèvre, O., et al. 2013, A&A, 556, 55
Ivison, R. J., Papadopoulos, P. P., Smail, I., et al. 2011, MNRAS, 412, 1913
Ivison, R. J., Magnelli, B., Ibar, E., et al. 2010, A&A, 518, L31
Kelson, D. D. 2003, PASP, 115, 688
Kochanek, C. S., Eisenstein, D. J., Cool, R. J., et al. 2012, ApJS, 200, 8
Kovács, A., Chapman, S. C., Dowell, C. D., et al. 2006, ApJ, 650, 592
Kroupa, P. 2002, Science, 295, 82
Michałowski, M. J., Dunlop, J. S., Cirasuolo, M., et al. 2012, A&A, 541, 85
Mo, H., van den Bosch, F. C., & White, S. 2010, Galaxy Formation and Evolution (Cambridge University Press)
Murphy, E. J., Condon, J. J., Schinnerer, E., et al. 2011, ApJ, 737, 67
Narayanan, D., Turk, M., Feldmann, R., et al. 2015, Nature, 525, 496
Nayyeri, H., Keele, M., Cooray, A., et al. 2016, ArXiv e-prints
Neistein, E., & Dekel, A. 2008, MNRAS, 383, 615
Nguyen, H. T., Schulz, B., Levenson, L., et al. 2010, A&A, 518, L5
Oke, J. B., Cohen, J. G., Carr, M., et al. 1995, PASP, 107, 375
Oliver, S. J., Bock, J., Altieri, B., et al. 2012, MNRAS, 424, 1614
Papovich, C., Cool, R., Eisenstein, D., et al. 2006, AJ, 132, 231
Perley, R. A., & Butler, B. J. 2013, ApJS, 204, 19
Prochaska, J. X., Hennawi, J. F., & Simcoe, R. A. 2013a, ApJ, 762, L19
Prochaska, J. X., Hennawi, J. F., Lee, K.-G., et al. 2013b, ApJ, 776, 136
Rahmati, A., Schaye, J., Bower, R. G., et al. 2015, MNRAS, 452, 2034
Rigby, E. E., Maddox, S. J., Dunne, L., et al. 2011, MNRAS, 415, 2336
Roseboom, I. G., Oliver, S. J., Kunz, M., et al. 2010, MNRAS, 409, 48
Scott, S. E., Dunlop, J. S., & Serjeant, S. 2006, MNRAS, 370, 1057
Seifert, W., Appenzeller, I., Baumeister, H., et al. 2003, in Proc. SPIE, Vol. 4841, Instrument Design and Performance for Optical/Infrared Ground-based Telescopes, ed. M. Iye & A. F. M. Moorwood, 962–973
Singh, P., Rana, S., Bagla, J. S., & Nath, B. B. 2016
Smail, I., Ivison, R. J., & Blain, A. W. 1997, ApJ, 490, L5
Smolčić, V., Aravena, M., Navarrete, F., et al. 2012, A&A, 548, A4
Swinbank, A. M., Smail, I., Longmore, S., et al. 2010, Nature, 464, 733
Tacchella, S., Dekel, A., Carollo, C. M., et al. 2015, ArXiv e-prints
Tacconi, L. J., Genzel, R., Smail, I., et al. 2008, ApJ, 680, 246
Targett, T. A., Dunlop, J. S., Cirasuolo, M., et al. 2012, arXiv:1208.3464
Toft, S., Smolčić, V., Magnelli, B., et al. 2014, ApJ, 782, 68
Vacca, W. D., Cushing, M. C., & Rayner, J. T. 2003, PASP, 115, 389
Valiante, E., Smith, M. W. L., Eales, S., et al. 2016, MNRAS, submitted
Viero, M. P., Asboth, V., Roseboom, I. G., et al. 2014, ApJS, 210, 22
Wang, L., Viero, M., Clarke, C., et al. 2014, MNRAS, 444, 2870
Wardlow, J. L., Smail, I., Coppin, K. E. K., et al. 2011, MNRAS, 415, 1479
Weiß, A., Kovács, A., Coppin, K., et al. 2009, ApJ, 707, 1201
White, M., Myers, A. D., Ross, N. P., et al. 2012, MNRAS, 424, 933
Yun, M. S., Scott, K. S., Guo, Y., et al. 2012, MNRAS, 420, 957